Journal of Alloys and Compounds 509 (2011) 3375–3381

Contents lists available at ScienceDirect

Journal of Alloys and Compounds

journal homepage: www.elsevier.com/locate/jallcom

Host-sensitized multicolor tunable luminescence of lanthanide ion doped one-dimensional YVO_4 nano-crystals

Ping Huang, Daqin Chen, Yuansheng Wang*

State Key Laboratory of Structural Chemistry, Fujian Institute of Research on the Structure of Matter, Chinese Academy of Sciences, Fuzhou, Fujian 350002, PR China

ARTICLE INFO

Article history:
Received 12 October 2010
Received in revised form 9 December 2010
Accepted 9 December 2010
Available online 16 December 2010

Keywords:
Optical materials
Optical properties
Optical spectroscopy
TEM
Nanorods

ABSTRACT

We report the Na_2EDTA-assisted synthesis of the lanthanide (Ln^{3+}) ion doped one-dimensional YVO_4 nanobelts and nanorods by a facile hydrothermal route. XRD, TEM, EDS and FTIR techniques are used to characterize the microstructures of the synthesized nano-crystals. The morphology-dependent luminescent behaviors of Eu^{3+}:YVO_4 are systematically investigated. Under a single wavelength UV light excitation, the Ln^{3+}:YVO_4 (Ln = Nd, Sm, Eu, Dy, Ho, Er, Tm, or Yb) nanorods exhibit visible to near-infrared (NIR) multicolor tunable luminescence via efficient host sensitization, while no emissions are detected for the Ce^{3+}, Pr^{3+}, or Tb^{3+} doped samples. Based on the results, possible mechanisms depicting the YVO_4 host sensitizing or quenching of lanthanide emissions are proposed.

© 2010 Elsevier B.V. All rights reserved.

1. Introduction

Recently, dramatic efforts have been dedicated to the elaboration of materials emitting multicolor tunable luminescence under a single wavelength excitation, for their important potential applications in the fields of light display, bio-labels and optoelectronic devices [1–3]. Among various luminescent materials, lanthanide ion (Ln^{3+}) activated phosphors have attracted extensive attention because of their wide range of emission colors and excellent luminescent performance. To achieve highly efficient multicolor tunable luminescence of lanthanide ions, host sensitization via energy transfer from the excited host to the Ln^{3+} ions is an effective way to overcome the low absorptions of parity forbidden 4f–4f transitions of Ln^{3+} [4–7]. Semiconductor nano-crystals (such as ZnO, In_2O_3, TiO_2, and SnO_2) have been considered as promising candidates for such hosts and sensitizers due to the ease to tailor their optical properties via size or morphology control [8–13]. However, owing to the necessary charge compensation or the unmatched radius between Ln^{3+} and cations of semiconductor, doping of high content of Ln^{3+} into the semiconductor nano-crystals is very tough [14].

Yttrium vanadate (YVO_4) crystal has been demonstrated to be a useful host and sensitizer for lanthanide ions to produce a variety of colors [15]. A typical sample is the Eu^{3+} ion doped yttrium vanadate (Eu^{3+}:YVO_4) powder, which has been widely used as red phosphor in cathode ray tubes (CRT) and color television for its high luminescence efficiency upon electron-beam excitation. Recently, several works have been extended to the Eu^{3+} doped nano-sized YVO_4 since inorganic nano-crystals have exhibited many fascinating novel size- and morphology-dependent properties [16–18]. Besides Eu^{3+}, Dy^{3+} or Sm^{3+} doped YVO_4 nano-crystals have also been investigated since Dy^{3+}:YVO_4 is a potential white phosphor due to the blue ($^4F_{9/2} \rightarrow {}^6H_{15/2}$) and yellow ($^4F_{9/2} \rightarrow {}^6H_{13/2}$) emissions of Dy^{3+}, and Sm^{3+}:YVO_4 yields characteristic orange-red luminescence originated from the $^4G_{5/2} \rightarrow {}^6H_J$ (J = 5/2, 7/2 and 9/2) transitions of Sm^{3+} [1]. In addition, by partial replacement of VO_4^{3-} by PO_4^{3-}, a new series of Ln^{3+} (Ln = Eu, Dy, Sm) doped yttrium phosphate–vanadate ($YV_{1-x}P_xO_4$) phosphors have been obtained with better optical properties [1,19,20]. Although the investigations on lanthanide ion doped YVO_4 and $YV_{1-x}P_xO_4$ nano-crystals are extensive, rare study has been focused on the synthesis and size- or morphology-dependent luminescence of the one-dimensional (1D) or quasi-one-dimensional (Q-1D) YVO_4 and $YV_{1-x}P_xO_4$ phosphors.

Herein, we report the Na_2EDTA-assisted synthesis of total group lanthanide ion doped YVO_4 1D nanobelts and nanorods by a facile hydrothermal route. Using Eu^{3+} ions as structural probe, the morphology-dependent luminescent behaviors of Eu^{3+}:YVO_4 are investigated. As a comparison, emissions of the irregular polyhedral nano-crystals and micro-crystals are also measured. In addition, the visible to near-infrared (NIR) multicolor tunable luminescence of the Ln^{3+}:YVO_4 nanorods via host sensitization under a single wavelength excitation are demonstrated, and the possible luminescent mechanisms are discussed.

* Corresponding author.
E-mail address: yswang@fjirsm.ac.cn (Y. Wang).

0925-8388/$ – see front matter © 2010 Elsevier B.V. All rights reserved.
doi:10.1016/j.jallcom.2010.12.069

Table 1
Summary of the synthesizing conditions as well as the corresponding morphologies and dimensions of the samples.

Sample	Synthesizing condition	Morphology	Diameter (nm)	Length (nm)
150EY	Hydrothermal treatment with the assistance of Na_2EDTA at 150 °C for 12 h, pH = 9.5	Nanobelt	3–8	300–500
180EY	Hydrothermal treatment with the assistance of Na_2EDTA at 180 °C for 12 h, pH = 9.5	Nanorod	15–20	200–300
PEY	Hydrothermal treatment with the assistance of $Na_3C_6H_5O_7$ at 180 °C for 12 h, pH = 12.5	Polyhedral nano-crystal	20–30	20–30
BEY	Solid-state reaction	Polyhedral micro-crystal	1500–2000	1500–2000

2. Experimental

2.1. Reagents

All the chemical reagents, i.e., yttrium nitrate hexahydrate ($Y(NO_3)_3{\cdot}6H_2O$), lanthanide nitrate hexahydrate ($Ln(NO_3)_3{\cdot}6H_2O$), disodium ethylenediamine tetraacetate (Na_2EDTA), sodium orthovanadate dodecahydrate ($Na_3VO_4{\cdot}12H_2O$), cetyltrimethyl ammonium bromide (CTAB), sodium citrate dihydrate ($Na_3C_6H_5O_7{\cdot}2H_2O$) and sodium hydroxide (NaOH) were of analytical grade, purchased from Sinopharm Chemical Reagent Co. and used without further purification.

2.2. Synthesis of 1D nano-crystals

The 5 mol% Ln^{3+}:YVO_4 1D nano-crystals were synthesized through a facile hydrothermal method with the assistance of Na_2EDTA. Firstly, $Y(NO_3)_3{\cdot}6H_2O$ (1.425 mmol) and $Ln(NO_3)_3{\cdot}6H_2O$ (0.075 mmol) were dissolved in 30 ml deionized water, then metal-chelating agent Na_2EDTA (1.5 mmol) was added to get a suspension. Secondly, $Na_3VO_4{\cdot}12H_2O$ (1.5 mmol) was dissolved in 30 ml deionized water, forming a solution which was then added drop-wise to the suspension under vigorous stirring to get a transparent yellow-colored mixture. Subsequently, pH of the mixture was carefully adjusted to 9.5 by the NaOH solution, followed by the addition of the surfactant CTAB (0.06 g) under vigorous stirring. Finally, the obtained mixture was poured into a Teflon-lined stainless steel autoclave, and heated at 180 °C for 12 h. As the autoclave was cooled down to room temperature, the product was collected by centrifugation, washed with deionized water and absolute ethanol for several times, and dried in vacuum at 60 °C for 24 h.

The pure YVO_4 nano-crystals were synthesized in a similar way. To investigate the morphology-dependent luminescence, Eu^{3+}:YVO_4 nano-crystals with different morphologies (denoted as 150EY and 180EY) were prepared by hydrothermal treating at 150 °C and 180 °C for 12 h, respectively.

2.3. Synthesis of polyhedral Eu^{3+}:YVO_4 nano-crystals

The polyhedral Eu^{3+}:YVO_4 nano-crystals (denoted as PEY) were synthesized with the assistance of $Na_3C_6H_5O_7$. $Y(NO_3)_3{\cdot}6H_2O$ (1.84 mmol) and $Eu(NO_3)_3{\cdot}6H_2O$ (0.40 mmol) were dissolved in 30 ml deionized water, which was then added to the 20 ml solution of metal-chelating agent $Na_3C_6H_5O_7{\cdot}2H_2O$ (1.57 mmol) to form the Y–Ln citrate suspension. In another vessel, $Na_3VO_4{\cdot}12H_2O$ (1.97 mmol) was dissolved in the 30 ml deionized water, and NaOH solution was added carefully to adjust pH to 12.5. The solution was then added drop-wise to the above suspension under vigorous stirring. After ageing at 90 °C for 30 min, the mixture was poured into a Teflon-lined stainless steel autoclave and heated at 180 °C for 12 h. As the autoclave was cooled down to room temperature, the product was collected by centrifugation, washed with deionized water and absolute ethanol for several times, and dried in vacuum at 60 °C for 24 h.

2.4. Synthesis of Eu^{3+}:YVO_4 micro-crystals

Eu^{3+}:YVO_4 micro-crystals (denoted as BEY) were prepared by solid-state reaction. The stoichiometric mixtures of Y_2O_3, NH_4VO_4 and Eu_2O_3 were ground together and heated in an alumina crucible at 650 °C for 24 h. The products were then removed from the furnace, cooled, finely ground and reheated at 850 °C for 48 h to complete the reaction.

A summary of the synthesizing conditions as well as the corresponding morphologies and dimensions of the samples is listed in Table 1.

2.5. Characterizations

X-ray diffraction (XRD) analyses on the products were carried out with a powder diffractometer (DMAX2500 RIGAKU) using CuK_α radiation (λ = 0.154 nm). The microstructures of the samples were studied using a transmission electron microscope (TEM, JEM-2010) equipped with an energy dispersive X-ray spectroscopy (EDS) system. The samples were ground into very fine powder that was placed onto a carbon-coated copper grid and introduced into the microscope. Fourier transform infrared (FTIR) spectra were measured on a Perkin-Elmer IR spectrometer using a KBr pellet technique. The emission, excitation spectra and decay curves of the as-prepared samples were recorded on an Edinburgh Instruments FLS920 spectrofluorometer equipped with both continuous (450 W) and pulsed xenon lamps. All the measurements were carried out at room temperature.

3. Results and discussion

3.1. Microstructure

XRD patterns of the as-synthesized samples are presented in Fig. 1. All the samples exhibit diffraction peaks that can be easily indexed by the tetragonal YVO_4 phase (JCPDS 17-0341). Compared with those of the micro-crystalline sample (BEY), the broader diffraction peak widths indicate the smaller grain sizes of the three hydrothermally prepared samples. Based on Scherrer equation, the mean grain size of the synthesized 150EY, 180EY and PEY samples are evaluated to be 12 nm, 40 nm and 28 nm, respectively.

TEM images of the Eu^{3+}:YVO_4 nano-crystals synthesized with the assistance of Na_2EDTA are presented in Fig. 2(a) and (c). The 150EY sample exhibits nanobelts with width ranging from 3 to 8 nm and length from 300 to 500 nm; while the 180EY one shows nanorods with diameter ranging from 15 to 20 nm and length from 200 to 300 nm. The PEY sample prepared with the help of $Na_3C_6H_5O_7$, as presented in Fig. 3(e), is irregular polyhedral nano-crystals sized 20–30 nm. Similarly, the micro-crystalline sample (BEY), shown in Fig. 3(g), are irregular polyhedral particles. However, the particle size is in the range of 1.5–2.0 μm. The corresponding selected area electron diffraction (SAED) patterns demonstrate that all the nanobelts, nanorods, polyhedral nanocrystals and microcrystals are tetragonal YVO_4, agreeing well with the XRD results. HRTEM images presented in Fig. 2(b), (d) and (f) verify the mono-crystalline nature of the nanobelt, nanorod and polyhedral nanoparticles. The formation of various morphologies for the synthesized nanocrystals might be determined by the combined roles of the chelating agent and pH value of the solution, similar to the cases previously reported by Lin et al. [21–23].

Fig. 3 shows the typical EDS spectra taken from Ce^{3+}:YVO_4, Nd^{3+}:YVO_4, Eu^{3+}:YVO_4 and Tb^{3+}:YVO_4 nanorods. Obviously, these nanorods consist of Y, V, O and Ln (Ce, Nd, Eu, or Tb) elements, indicating that Ln^{3+} ions are doped into the YVO_4 nano-crystals.

FTIR spectra of the nanobelts, nanorods, and micro-crystals are displayed in Fig. 4. The intense peak at about 800 cm^{-1} is apparently associated with the characteristic vibrational mode of

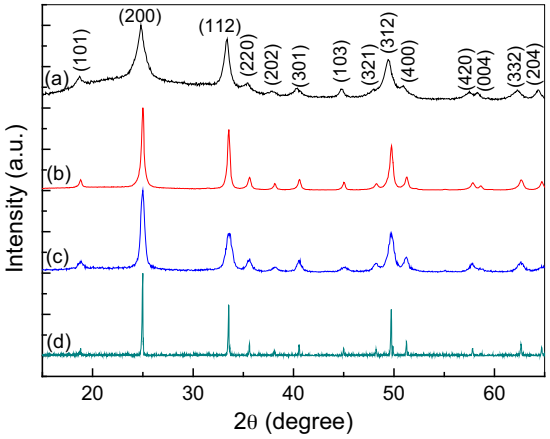

Fig. 1. XRD patterns of as-synthesized samples: (a) 150EY, (b) 180EY, (c) PEY and (d) BEY.

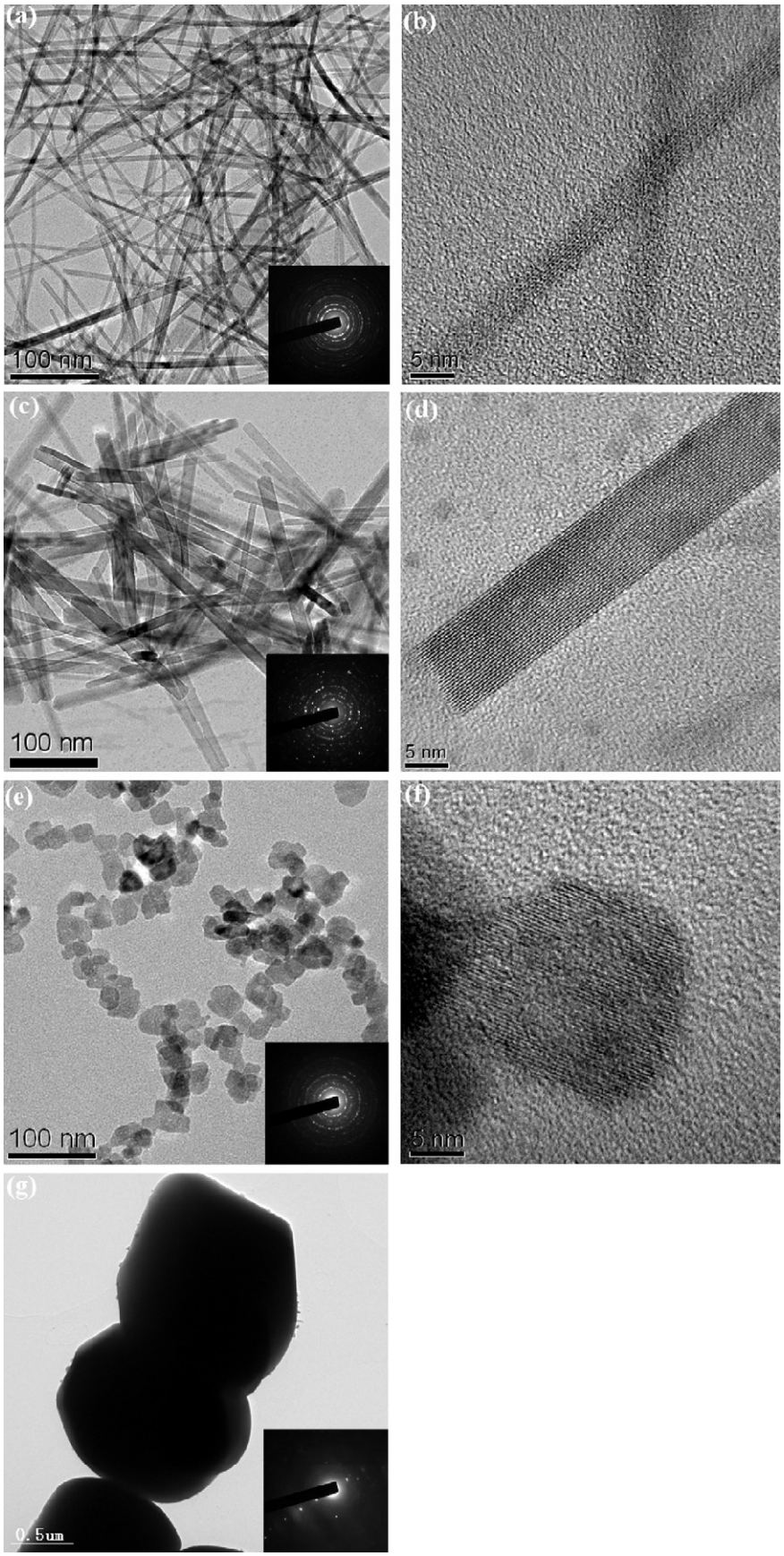

Fig. 2. Typical TEM images and corresponding SAED patterns of (a) Eu^{3+}:YVO_4 nanobelts (150EY), (c) nanorods (180EY), (e) polyhedral nano-crystalline (PEY) and (g) micro-crystalline samples (BEY); (b), (d), and (f) show HRTEM images of nanobelt, nanorod and polyhedral nano-crystals in (a), (c) and (e).

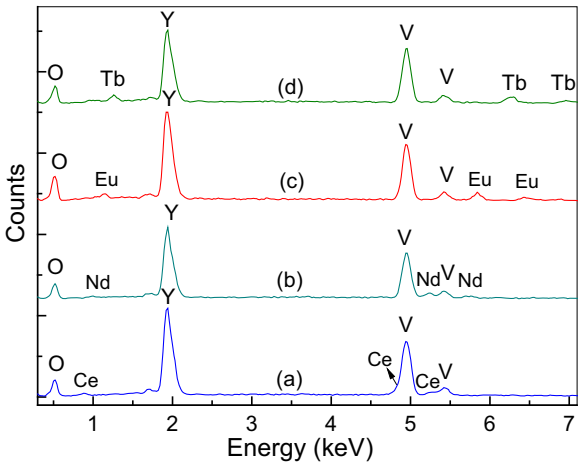

Fig. 3. EDS spectra of (a) Ce^{3+}:YVO_4, (b) Nd^{3+}:YVO_4, (c) Eu^{3+}:YVO_4 and (d) Tb^{3+}:YVO_4 nanorods.

V–O bond for all the samples [24,25]. However, compared with that of the micro-crystals, the vibrational peaks of V–O bonds of the nanobelts and nanorods are obviously broadened. The broad absorption band at 3420 cm^{-1} and a weak one at 1610 cm^{-1} are assigned to the symmetrical stretching vibration and the bending vibration of H–O–H (H_2O molecules), respectively. The peak at 1396 cm^{-1} is assigned to the vibration of the carboxylate anion. In addition, two weak bands at 2850 cm^{-1} and 2931 cm^{-1} correspond to the symmetrical and asymmetrical stretching vibrational modes of the CH_2 group, respectively. However, these vibrational organic groups are not detected in the micro-crystalline sample.

3.2. Morphology-dependent luminescence

The photoluminescence excitation (PLE) spectra for the 616 nm emission corresponding to Eu^{3+}:$^5D_0 \rightarrow {}^7F_2$ transition of the Eu^{3+}:YVO_4 nanobelts, nanorods and micro-crystals are presented in Fig. 5. All the excitation spectra consist of an intense broadband ranging from 200 to 350 nm and several weak narrow bands in the range of 350–550 nm. The broadband is originated from the O^{2-}–V^{5+} charge transfer (CT) within VO_4^{3-} group, which confirms that the emission of Eu^{3+} is ascribed to the efficient energy transfer from the excited VO_4^{3-} groups. Interestingly, the peak position of the O^{2-}–V^{5+} CT band red-shifts gradually with the grain morphology changing from nanobelt to nanorod and finally to micrometer-sized polyhedral particle, due to the effect of nano-size on the energy gap width of the CT band of the material.

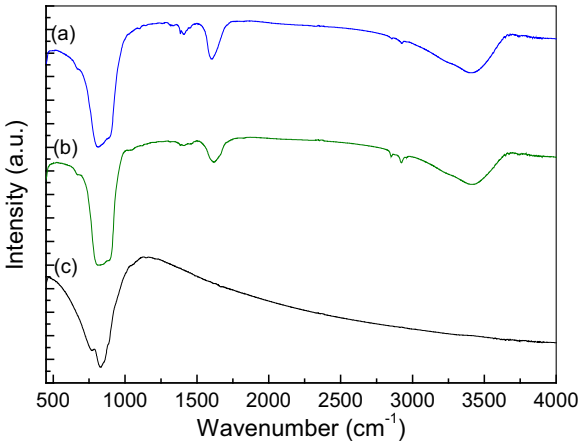

Fig. 4. FTIR spectra of (a) 150EY, (b) 180EY, and (c) BEY samples.

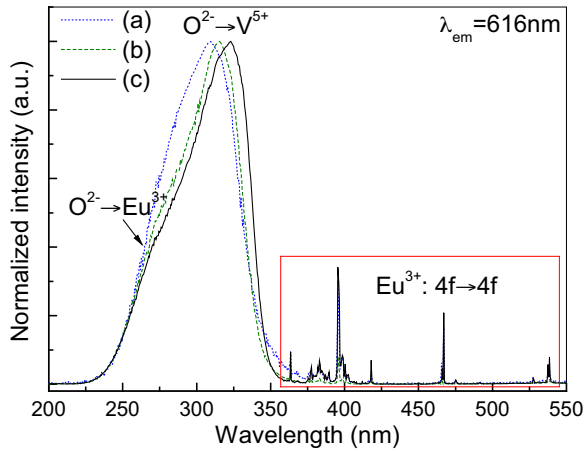

Fig. 5. Photoluminescence excitation (PLE) spectra of (a) 150EY, (b) 180EY and (c) BEY samples for the Eu^{3+}:$^5D_0 \rightarrow {}^7F_2$ emission.

The photoluminescence (PL) spectra of 150EY, 180EY, BEY and PEY samples under 310 nm excitation are shown in Fig. 6. When irradiated by 310 nm light, the electrons are excited from the ground state to the excited state of VO_4^{3-}, and then relax rapidly to the Eu^{3+}:$^5D_{1,2,3}$ states. The emissions are generated by the subsequent radiative transitions from the $^5D_0$ excited state to the ^7F_J (J = 1, 2, 3, 4) ones. It is well known that YVO_4 has the xenotime structure, which offers Y^{3+} ions the lattice site with a D_{2d} point symmetry. The main emission band around 616 nm originated from the $^5D_0 \rightarrow {}^7F_2$ electronic dipole transition is a consequence of the absence of the inversion symmetry of Eu^{3+} substituting Y^{3+} in YVO_4 [26]. Notably, the dominant Stark-splitting peak of the one-dimensional nano-crystals is located at 616 nm, while that of the irregular polyhedral nano-crystals or micro-crystals at 619 nm. The change in the relative intensity of the two Stark-splitting peaks is attributed to the difference of the effect of the crystal field perturbation on the individual f–f transition.

The luminescence decay curves of the Eu^{3+}:$^5D_0$ levels in different samples are exhibited in Fig. 7. The Eu^{3+}:$^5D_0$ lifetimes in the nanobelts (150EY) and nanorods (180EY) are determined to be 0.21 and 0.92 ms, respectively. Compared with that of the

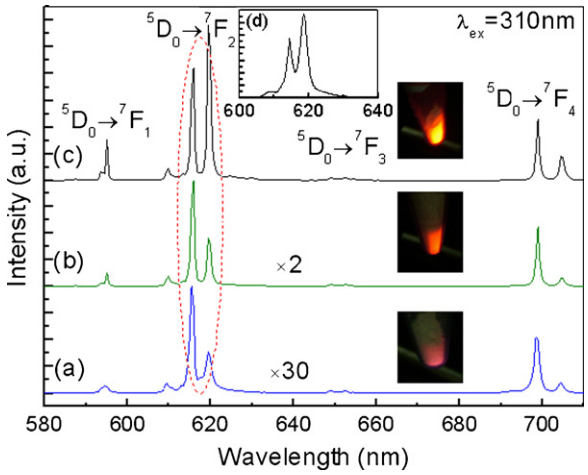

Fig. 6. Photoluminescence (PL) spectra of (a) 150EY, (b) 180EY, (c) BEY, and (d) PEY samples under 310 nm excitation; insets show the luminescence photographs of 150EY, 180EY and BEY samples respectively.

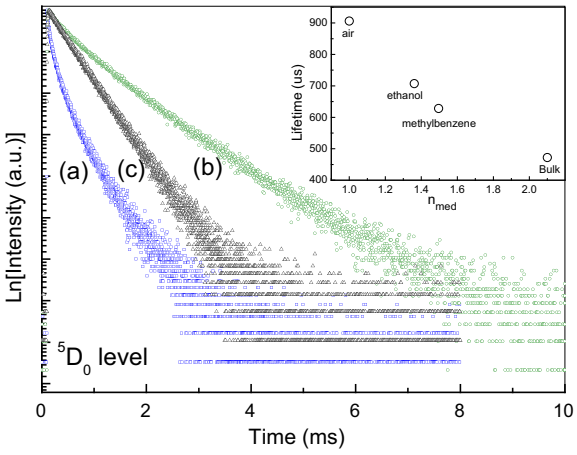

Fig. 7. The luminescence decay curves of Eu^{3+}:$^5D_0$ levels for (a) 150EY, (b) 180EY, and (c) BEY samples under 310 nm excitation; inset shows the dependence of the $^5D_0$ lifetime of Eu^{3+}in YVO_4 nanorods on the refractive index of the surrounding medium.

nanorods, the nanobelts have higher surface to volume ratio, and correspondingly, more surface defects which promote the non-radiative relaxation, resulting in shorter Eu^{3+} lifetime. Interestingly, the Eu^{3+}:$^5D_0$ lifetime in 180EY is significantly longer than that in the BEY sample (0.48 ms), attributing probably to the non-solid medium surrounding the nano-crystals which changes the effective refractive index and thus the radiative lifetime, similar to the cases previously reported in the Ln^{3+} doped LaF_3 and Gd_2O_3 nano-crystals [27,28]. It is well known that the radiative lifetime τ_r is dependent on the refractive index n: $\tau_r \infty (1/f)(\lambda_0^2/\chi)$, where $\chi = n[(n^2+2)/3]^2$ for electronic dipole transitions, f the oscillator strength, λ_0 the wavelength in vacuum [28]. For nano-crystals, n should be replaced by the effective refractive index n_{eff}, where $n_{eff} = xn_{nc} + (1-x)n_{med}$, x is the filling factor showing what fraction of space is filled by nano-crystals with a refractive index n_{nc}, and n_{med} the refractive index of the medium. In order to reveal the influence of the surrounding medium on the radiative lifetime of the nano-crystals, the fluorescence lifetime of Eu^{3+}:$^5D_0$ in the nanorods immersed in liquids with different refractive indices were measured, as shown in the inset of Fig. 7. Obviously, the lifetime

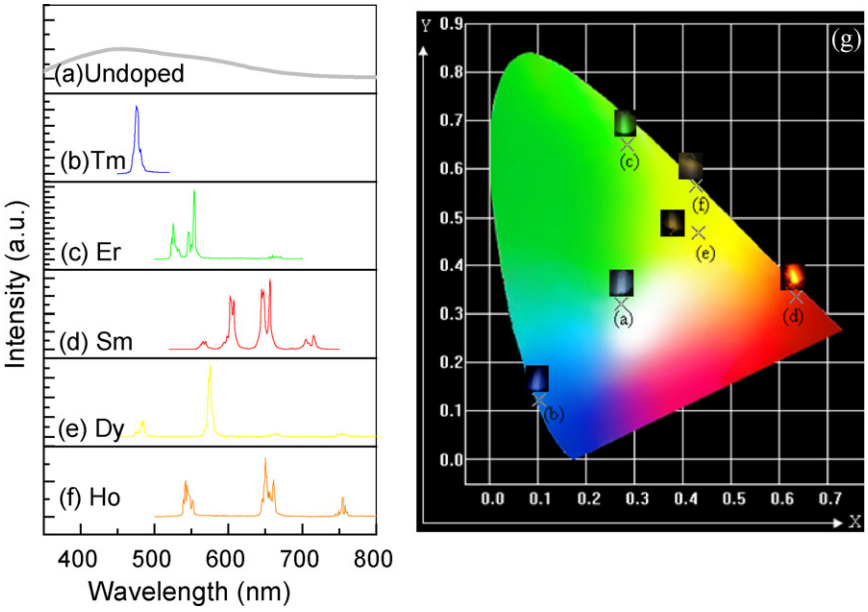

Fig. 8. Visible PL spectra of (a) pure, (b) Tm^{3+}, (c) Er^{3+}, (d) Sm^{3+}, (e) Dy^{3+}, and (f) Ho^{3+} doped YVO_4 nanorods; (g) CIE (X, Y) coordinate diagram showing the corresponding luminescent chromaticity points of Ln^{3+} doped YVO_4 nanorods.

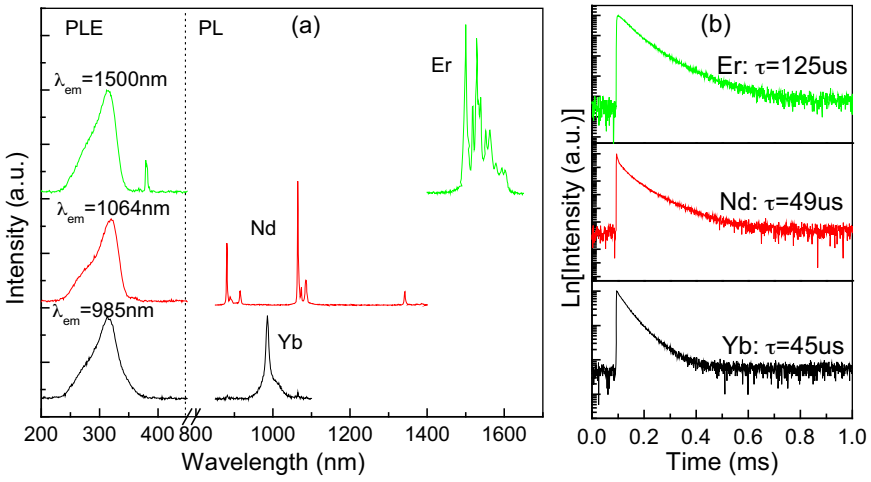

Fig. 9. (a) Near-infrared PL and PLE spectra and (b) decay curves of Er^{3+}, Nd^{3+} and Yb^{3+} doped YVO_4 nanorods.

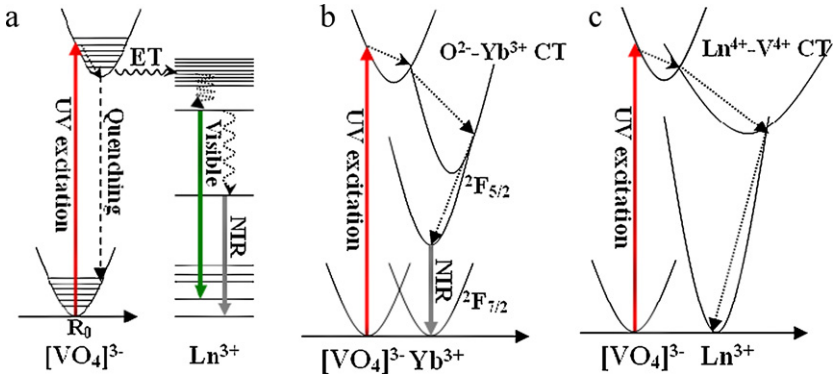

Fig. 10. Energy transfer (ET) mechanisms describing the YVO_4 host sensitizing or quenching of Ln^{3+} emissions. (a) Ln = Nd, Sm, Dy, Ho, Er, Tm; (b) Ln = Yb; and (c) Ln = Ce, Pr, Tb. The dotted arrows denote multi-phonon non-radiative transitions, the straight ones denote radiative transitions, and CT denotes charge transfer state.

is significantly affected by the surrounding medium. The larger refractive index of the surrounding medium leads to the shorter lifetime. Therefore, the measured longer lifetime of Eu^{3+}:$^5D_0$ in the YVO_4 nanorods is due to the low refractive index of air surrounding the sample.

3.3. Host-sensitized multi-color tunable luminescence

To demonstrate the emission versatility of the as-synthesized YVO_4 nanorods, PL and PLE spectra of the various Ln^{3+} doped YVO_4 (Ln = Ce, Pr, Nd, Sm, Tb, Dy, Ho, Er, Tm, Yb) nano-crystals were recorded, as shown in Figs. 8 and 9. For the pure YVO_4, a broadband emission covering the whole visible region is observed, which might be originated from the defect centers since it is proved that the excited energy in the pure YVO_4 crystal will transfer easily to a quenching site through the VO_4^{3-} groups and dissipate non-radiatively, therefore no visible emission can be detected at room temperature [29]. When Ln^{3+} ions are doped into YVO_4, Ln^{3+} ions act as the activators to induce the characteristic emissions through efficient energy transfer from the excited state of VO_4^{3-} to the activators. Interestingly, except Ce^{3+}, Pr^{3+} and Tb^{3+}, all the other Ln^{3+} ion doped YVO_4 nanorods exhibit visible or NIR emissions. As shown in Fig. 8, under 310 nm excitation corresponding to the VO_4^{3-} group absorption, sharp emissions assigned respectively to the $^1G_4 \rightarrow {}^3H_6$ (blue), $^2H_{11/2}$, $^4S_{3/2}$, $^4F_{9/2} \rightarrow {}^6H_{5/2}$ (green), $^4G_{5/2} \rightarrow {}^6H_{5/2,7/2,9/2,11/2}$ (orange), $^4F_{9/2} \rightarrow {}^6H_{15/2,13/2,11/2}$ (yellow), and $^5F_4$, $^5F_5$, $^5I_4 \rightarrow {}^5I_8$ (yellow) transitions are observed in the Tm^{3+}, Er^{3+}, Sm^{3+}, Dy^{3+} or Ho^{3+} doped samples. The corresponding visible emission spectra of the nanorods doped with various Ln^{3+} ions can be easily converted to the Commission International de l'Eclairage (CIE) 1931 chromaticity diagram, as plotted in Fig. 8(g).

In addition to the visible luminescence, the YVO_4 nanorods doped with appropriate Ln^{3+} ions such as Er^{3+}, Nd^{3+} or Yb^{3+} also exhibit near-infrared emissions with the help of host-sensitization of YVO_4, as presented in Fig. 9(a). The emissions originated from Er^{3+}:$^4I_{13/2} \rightarrow {}^4I_{15/2}$, Nd^{3+}:$^4F_{3/2} \rightarrow {}^4I_{9/2,11/2,13/2}$ and Yb^{3+}:$^2F_{5/2} \rightarrow {}^2F_{7/2}$ transitions cover the whole NIR region between 850 and 1650 nm. The corresponding excitation spectra evidenced the efficient energy transfer from the excited state of VO_4^{3-} to the NIR emission activators. All the lifetime curves of the Er^{3+}:$^4I_{13/2}$, Nd^{3+}:$^4F_{3/2}$, and Yb^{3+}:$^2F_{5/2}$ levels, shown in Fig. 9(b), exhibit the non-exponential decay behaviors, which is ascribed to the influence of surface defects of nanorods on the Ln^{3+} radiative transitions. The effective lifetimes were estimated to be 125, 49 and 45 μs, respectively, by the formula $\tau_{eff} = \int I(t)tdt / \int I(t)dt$, where $I(t)$ represents the luminescent intensity at time t.

3.4. Host-to-Ln^{3+} sensitization mechanisms

The possible mechanisms depicting the YVO_4 host sensitizing or quenching of Ln^{3+} emissions are illustrated in Fig. 10. Under UV excitation, the VO_4^{3-} groups are excited from the ground state to the excited one. When energy matching condition is met, the excited VO_4^{3-} may serve as a universal sensitizer for a wide range of Ln^{3+} activators such as Nd^{3+}, Sm^{3+}, Dy^{3+}, Ho^{3+}, Er^{3+} and Tm^{3+}. After non-radiative relaxation to the metastable excited states, these Ln^{3+} ions emit visible or NIR light, as shown in Fig. 10(a). As for the sensitizing emission of Yb^{3+}, the energy transfer process can occur only with the help of the O^{2-}–Yb^{3+} charge transfer (CT) state, since the energy gap between the unique excited state Yb^{3+}:$^2F_{5/2}$ and the VO_4^{3-} state is about 30,000 cm^{-1}, being too large to be matched by phonons. As exhibited in Fig. 10(b), the electrons in VO_4^{3-} group are firstly transferred to the O^{2-}–Yb^{3+} CT state, then non-radiatively relax to the Yb^{3+}:$^2F_{5/2}$ excited state from which the NIR emission is generated. For Ce^{3+}, Pr^{3+} and Tb^{3+}, it is well known that they have a great tendency to be oxidized to quadrivalence, while V^{5+} ions have a tendency to be reduced, forming the Ln^{4+}–V^{4+} CT state [15]. Therefore, the excited electrons are easily transferred to the Ln^{4+}–V^{4+} CT state followed by the non-radiative relaxation to the ground states of Ln^{3+}, resulting in the quenching of Ln^{3+} emissions, as shown in Fig. 10(c).

4. Conclusions

In summary, the lanthanide ion doped one dimensional YVO_4 nanobelts and nanorods were prepared, and their morphology-dependent luminescence was studied. Evidently, the excitation, emission and decay behaviors of Eu^{3+}:YVO_4 nanorods are quite different from those of the micro-crystalline samples. Under UV excitation, visible to near-infrared multicolor tunable luminescence of Ln^{3+}:YVO_4 (Ln = Nd, Sm, Eu, Dy, Ho, Er, Tm, or Yb) nanorods are achieved via efficient energy transfer from the excited VO_4^{3-} groups to the lanthanide activators.

Acknowledgements

This work was supported by the National Natural Science Foundation of China (50902130, 10974201), the Natural Science Foundation of Fujian Province (2009J05139), and the Key Lab of Optelectronic Materials Chemistry and Physics, CAS (2008DP173016).

References

[1] F. Wang, X. Xue, X.G. Liu, Angew. Chem. Int. Ed. 47 (2008) 906.
[2] F. Wang, X.G. Liu, J. Am. Chem. Soc. 130 (2008) 5642.

[3] Y.S. Liu, D.T. Tu, H.M. Zhu, R.F. Li, W.Q. Luo, X.Y. Chen, Adv. Mater. 22 (2010) 3266.
[4] D.Q. Chen, Y.L. Yu, P. Huang, H. Lin, Z.F. Shan, L.W. Zeng, A.P. Yang, Y.S. Wang, Phys. Chem. Chem. Phys. 12 (2010) 7775.
[5] X.M. Liu, C.K. Lin, J. Lin, Appl. Phys. Lett. 90 (2007) 081904.
[6] R.X. Yan, Y.D. Li, Adv. Funct. Mater. 15 (2005) 763.
[7] C.X. Li, J. Yang, P.P. Yang, H.Z. Lian, J. Lin, Chem. Mater. 20 (2008) 4317.
[8] R. Krishna, D. Haranath, S.P. Singh, H. Chander, A.C. Pandey, D. Kanjilal, J. Mater. Sci. 42 (2007) 10047.
[9] Y.P. Du, Y.W. Zhang, L.D. Sun, C.H. Yan, J. Phys. Chem. C 112 (2008) 12234.
[10] J. Vela, B.S. Prall, P. Rastogi, D.J. Werder, J.L. Casson, D.J. Williams, V.I. Klimov, J.A. Hollingsworth, J. Phys. Chem. C 112 (2008) 20246.
[11] W.Q. Luo, R.F. Li, G.K. Liu, M.R. Antonio, X.Y. Chen, J. Phys. Chem. C 112 (2008) 10370.
[12] C.Y. Fu, J.S. Liao, W.Q. Luo, R.F. Li, X.Y. Chen, Opt. Lett. 33 (2008) 953.
[13] A. Kar, A. Patra, J. Phys. Chem. C 113 (2009) 4375.
[14] A.A. Bol, R. van Beek, A. Merjerink, Chem. Mater. 14 (2002) 1121.
[15] G. Blasse, B.C. Grabmaier, Luminescent Materials, Springer, Berlin, 1994.
[16] M. Haase, K. Riwotzki, H. Meyssamy, A. Kornowski, J. Alloys Compd. 303 (2000) 191.
[17] A. Huignard, V. Buissette, G. Laurent, T. Gacoin, J.P. Boilot, Chem. Mater. 14 (2002) 2264.
[18] C.H. Yan, L.D. Sun, C.S. Liao, Appl. Phys. Lett. 82 (2003) 3511.
[19] C.C. Wu, K.B. Chen, C.S. Lee, T.M. Chen, B.M. Cheng, Chem. Mater. 19 (2007) 3278.
[20] Z.Y. Hou, P.P. Yang, C.X. Li, L.L. Wang, H.Z. Lian, Z.W. Quan, J. Lin, Chem. Mater. 20 (2008) 6686.
[21] C.X. Li, Z.Y. Hou, C.M. Zhang, P.P. Yang, G.G. Li, Z.H. Xu, Y. Fang, J. Lin, Chem. Mater. 21 (2009) 4598.
[22] C.X. Li, Z.W. Quan, J. Yang, P.P. Yang, J. Lin, Inorg. Chem. 46 (2007) 6329.
[23] J. Yang, C.X. Li, Z.Y. Cheng, X.M. Zhang, Z.W. Quan, C.M. Zhang, J. Lin, J. Phys. Chem. C 111 (2007) 18148.
[24] M. Yu, J. Lin, J. Fang, Chem. Mater. 17 (2005) 1783.
[25] M.L. Pang, J. Lin, M. Yu, S.B. Wang, J. Solid State. Chem. 177 (2004) 2237.
[26] G. Jia, Y.H. Song, M. Yang, Y.J. Huang, L.H. Zhang, H.P. You, Opt. Mater. 31 (2009) 1032.
[27] J.W. Stouwdam, F.C.J.M. van Veggel, Nano Lett. 2 (2002) 733.
[28] L.Q. Liu, X.Y. Chen, Nanotechnology 18 (2007) 255704.
[29] Y.G. Su, G.S. Li, X.B. Chen, J.J. Liu, L.P. Li, Chem. Lett. 37 (2008) 762.